small
methods

Layered Electrodes Based on 3D Hierarchical Porous Carbon and Conducting Polymers for High-Performance Lithium-Sulfur Batteries

Shuaibo Zeng, Xin Li, Hai Zhong, Shaowei Chen,* and Yaohua Mai*

Easy dissolution of polysulfides and low loading of active materials are two major factors that limit the cathode cycling stability and energy density in lithium-sulfur batteries. Herein, 3D hierarchical carbon with abundant pores is used for sulfur encapsulation (S@DHPC), which achieves a high sulfur content of 74 wt% and high sulfur loading of 5.8 mg cm^{-2}. Importantly, coating the obtained S@DHPC electrode with poly(3,4-ethylenedioxythiophene)-poly(styrenesulfonate) (PEDOT:PSS) conducting polymers is found to effectively impede the diffusion of polysulfide species, leading to marked improvement of the cycling stability of the electrode; and the electrode performance increases with an increasing number of the S@DHPC/PEDOT:PSS layer. For a three-layer electrode, at a current density of 2 C, it delivers a discharge capacity of 846 mAh g^{-1} in the first cycle and maintains a capacity of 716 mAh g^{-1} after 500 cycles, corresponding to a fading rate of only 0.033% cycle^{-1}. Results from this study suggest that layered electrodes can be exploited as a unique electrode architecture for the fabrication of high-performance lithium-sulfur batteries.

1. Introduction

Lithium-sulfur (Li-S) batteries have been attracting much attention as an effective energy storage device due to their exceptional theoretical capacity (1672 mAh g^{-1}) and specific energy density (2600 Wh kg^{-1}), as compared to state-of-the-art lithium-ion batteries.[1] However, the practical application of Li-S batteries is severely impeded by several critical issues:[2] (i) loss of active materials during discharge, where intermediate species of long-chain lithium polysulfides (ranging from Li_2S_4 to Li_2S_8) can be readily dissolved into ether-based electrolytes;[3] (ii) low electrical conductivity of elemental sulfur and polysulfide intermediates;[4] (iii) large volumetric expansion during discharge;[5] and (iv) formation of lithium dendrites on the

anodal surface during charge–discharge processes.[6] These can lead to continuous and rapid capacity decay, low discharge capacities, and concerns of device safety.[7]

Substantial efforts have therefore been devoted to the mitigation of these challenges.[8] For instance, carbon/sulfur and polymer/sulfur composites have been prepared in recent years as two types of new cathode materials. Of these, porous carbon hosts, such as hollow carbon spheres,[9] carbon nanosheets,[10] carbon nanotubes,[11] nitrogen-doped carbon,[12] layered carbon matrices,[13] carbon nanofibers,[14] and graphene,[15] are of particular interest, as they can not only improve sulfur utilization via uniform dispersion of sulfur particles and enhanced cathode conductivity[16] but also confine sulfur and/or polysulfides on their large internal surfaces,[17] redeposit reaction intermediates, and mitigate polysulfide diffusion.[18] In addition, unique frameworks with well-defined structures, such as core–shell,[19] yolk-shell,[20] layer,[2a,4,21] and sandwich-type,[2a,22] have been utilized to substantially increase sulfur loading and impede the loss of active materials, an effective strategy to improve the battery performance. Nevertheless, with these carbon/sulfur frameworks, the cycling stability of Li-S batteries remains unsatisfactory because the encapsulation of sulfur is not sufficiently strong to totally eliminate the dissolution of polysulfides.[23] To mitigate this issue, polymers/sulfur composites have been prepared as cathode materials.[24] In particular, electrodes based on layers of soft polymers have been found to accommodate the large volume change and concurrently impede polysulfide dissolution during cycling.[25] The formation of chemical bonds between sulfur and the polymer backbone can further reduce the dissolution and diffusion of polysulfides.[26] However, sulfur-rich copolymers are mostly insulating, where the low conductivity limits the rate-capacity improvement,[27] and Li-S batteries using a single coating layer of polymers typically show a low sulfur loading (<2 mg cm^{-2}), and hence a low energy density.[28]
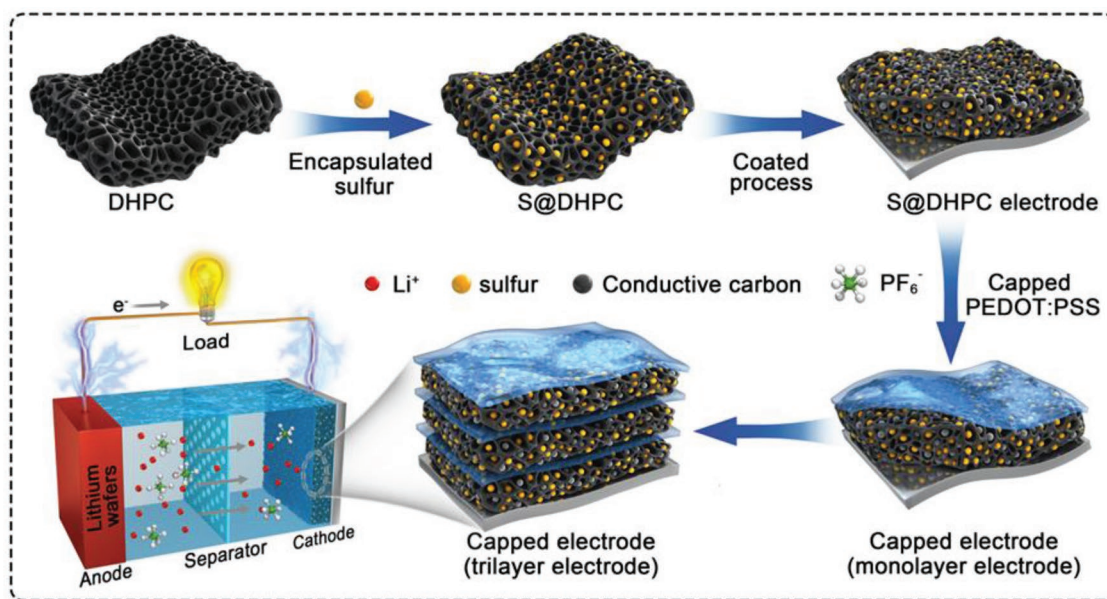
To simultaneously achieve high sulfur loading and good cycling stability, in this work, we successfully synthesized a three-dimensional (3D) hierarchical porous carbon (DHPC) as the sulfur host. After injection of sulfur, the resulting S@DHPC electrode was then coated with PEDOT:PSS conducting polymers. An electrode consisting of three stacks of S@DHPC/PEDOT:PSS was found to possess a high sulfur

Dr. S. B. Zeng, X. Li, Dr. H. Zhong, Prof. Y. H. Mai
Institute of New Energy Technology
College of Information Science and Technology
Jinan University
Guangzhou 510006, China
E-mail: yaohuamai@jnu.edu.cn
Prof. S. W. Chen
Department of Chemistry and Biochemistry
University of California
1156 High Street, Santa Cruz, CA 95064, USA
E-mail: shaowei@ucsc.edu

The ORCID identification number(s) for the author(s) of this article can be found under https://doi.org/10.1002/smtd.201900028.

ADVANCED
SCIENCE NEWS
www.advancedsciencenews.com

small
methods
www.small-methods.com

Figure 1. Schematic of the preparation of S@DHPC/PEDOT:PSS layered electrodes.

content (74 wt%) and sulfur loading (5.8 mg cm^{-2}) and deliver a specific capacity of 1420 mAh g^{-1} at 0.1 C and 626 mAh g^{-1} at 5 C. Moreover, the electrode retained a reversible capacity of 716 mAh g^{-1} even after 500 cycles, corresponding to a fading rate of only 0.033% cycle^{-1}. The excellent cycling performance was attributed to the conducting polymer films that prevented the diffusion/dissolution of polysulfides.

2. Results and Discussion

The preparation of the layered electrodes is schematically depicted in **Figure 1**. First, DHPC was fabricated by an oxidative template assembly route and used as an encapsulation matrix for sulfur loading. The 3D, poriferous, and interconnected structure of DHPC not only provided continuous pathways for electron transport but also large and internal volumes for the accommodation of sulfur. Additionally, the unique porous structure could greatly impede the diffusion of polysulfides into the electrolyte by the complex inner barriers. To obtain sulfur-carbon composite materials, sulfur and DHPC were mixed and thermally treated in an autoclave, where melted sulfur was infiltrated into the cavities of DHPC under the autogenerated pressure. To inhibit the diffusion of polysulfides, we coated the electrode surface with highly conductive PEDOT:PSS films as a physical barrier. The number of S@DHPC/PEDOT:PSS layers was varied by repeating the casting and coating process.

The microstructure and morphology of sulfur powders, DHPC, and layered electrodes were first characterized by scanning electron microscopy (SEM) and transmission electron microscopy (TEM) measurements. It can be seen that pure sulfur exhibited a uniform and granular structure (**Figure 2**a), with the particle size of hundreds of nanometers, whereas DHPC showed a poriferous, interconnected, and graphene-like structure (Figure 2b) that is beneficial for the encapsulation of active sulfur. In fact,

the corresponding Brunauer–Emmett–Teller (BET) surface area and total pore volume of DHPC are estimated to be 1828 m^2 g^{-1} and 2.17 cm^3 g^{-1} (Figure S1a, Supporting Information), respectively, with the pore size centered around 2.5 nm (Figure S1b, Supporting Information), which diminished markedly to 64 m^2 g^{-1}, 0.17 cm^3 g^{-1}, and 1.2 nm after sulfur encapsulation (Figure S1c,d, Supporting Information). SEM studies of S@DHPC further confirmed that sulfur was successfully infiltrated into the cavities of DHPC (Figure 2c). In order to better resolve the multilayer structure, we carried out SEM studies of the cross section of the trilayer electrode before rolling (Figure 2d), where the thickness was estimated to be ≈300 μm. After rolling of the electrode, SEM studies showed no observable delamination but the electrode thickness was found to decrease to ≈100 μm, indicating good contact at the interface between layers (Figure S2, Supporting Information). The corresponding elemental maps of the electrode are shown in Figure 2e–h, where sulfur, oxygen, and carbon can be readily identified throughout the entire electrode, suggesting a rather homogeneous distribution of active sulfur within the electrode. Note that the uniform distribution of sulfur and carbon is propitious to maximize sulfur loading by taking full advantage of the porous carbon structure.

The sulfur content in the S@DHPC sample was then quantified by thermogravimetric analysis (TGA) and X-ray photoelectron spectroscopy (XPS) measurements. **Figure 3**a depicts the TGA curve of the S@DHPC sample, where an apparent weight loss of ≈74% can be observed to occur from 150 to 400 °C, due to the evaporation of sulfur in the sample.[29] Consistent results were obtained in XPS measurements. From the XPS survey spectrum in Figure 3b, the sulfur content was estimated to be 75 wt%, based on the integrated peak areas of the S 2p (162.6 eV) and C 1s electrons (283.8 eV). In X-ray diffraction (XRD) measurements, the S@DHPC sample showed a series of sharp peaks at 23.1°, 25.8°, and 27.7°, consistent with those of crystalline sulfur (PDF No. 08-0247),[29] again,
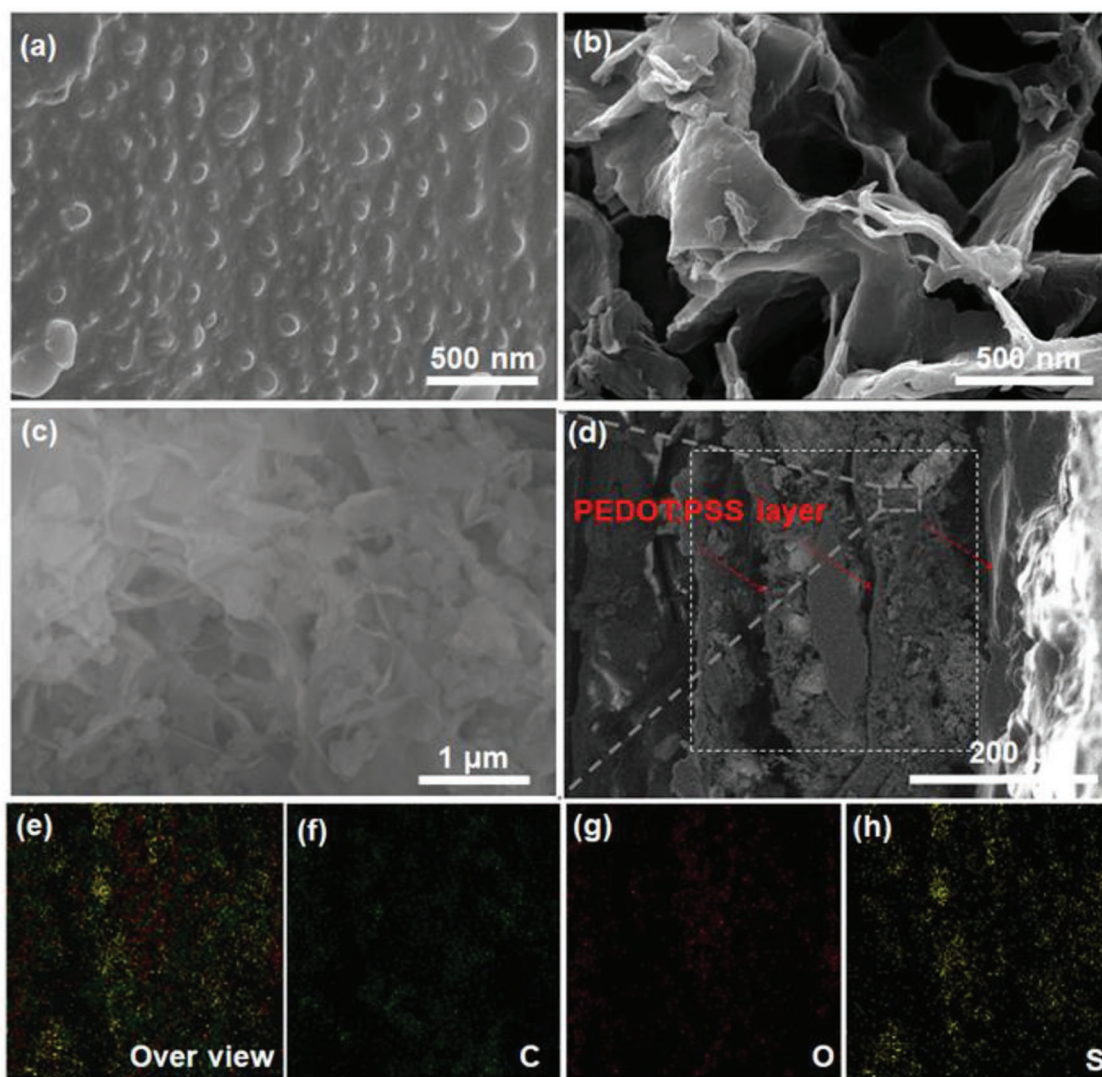
Figure 2. a–c) SEM images of S, DHPC, and S@DHPC; d) SEM images of the cross section of the S@DHPC/PEDOT:PSS trilayer electrode. Corresponding elemental maps of the rectangular area in panel (d), e) overall view, f) C, g) O, and h) S.

suggesting the successful infiltration of active sulfur into the carbon matrix (Figure 3c). Raman spectra of the DHPC and S@DHPC samples are shown in Figure S3 (Supporting Information). The ratio of the D and G band intensities (I_D/I_G) of

DHPC was estimated to be 1.01, which clearly demonstrates a high degree of graphitization of the sample.

To demonstrate practicality of the obtained materials for Li-S battery electrodes, a button-type Li-S battery with a
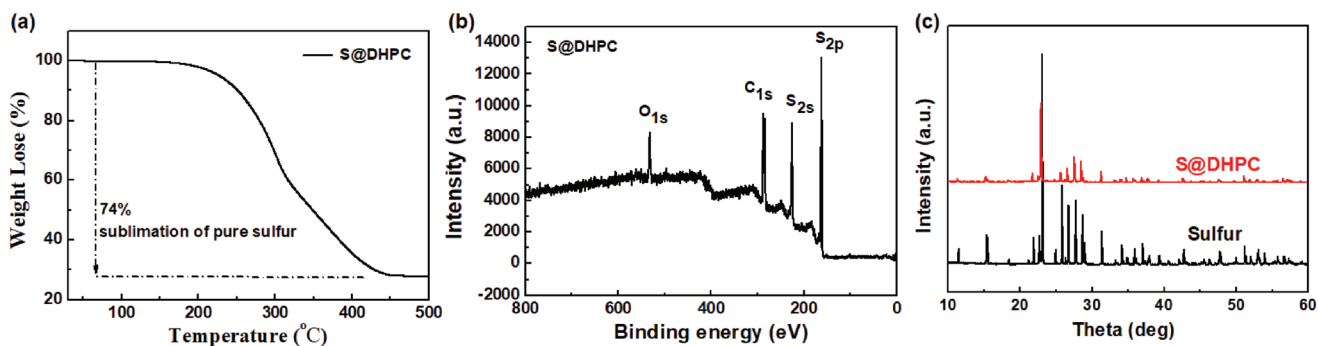
Figure 3. a) TGA curve of S@DHPC sample under an inert atmosphere. b) XPS survey spectrum of the S@DHPC composite. c) XRD patterns of sulfur and S@DHPC.
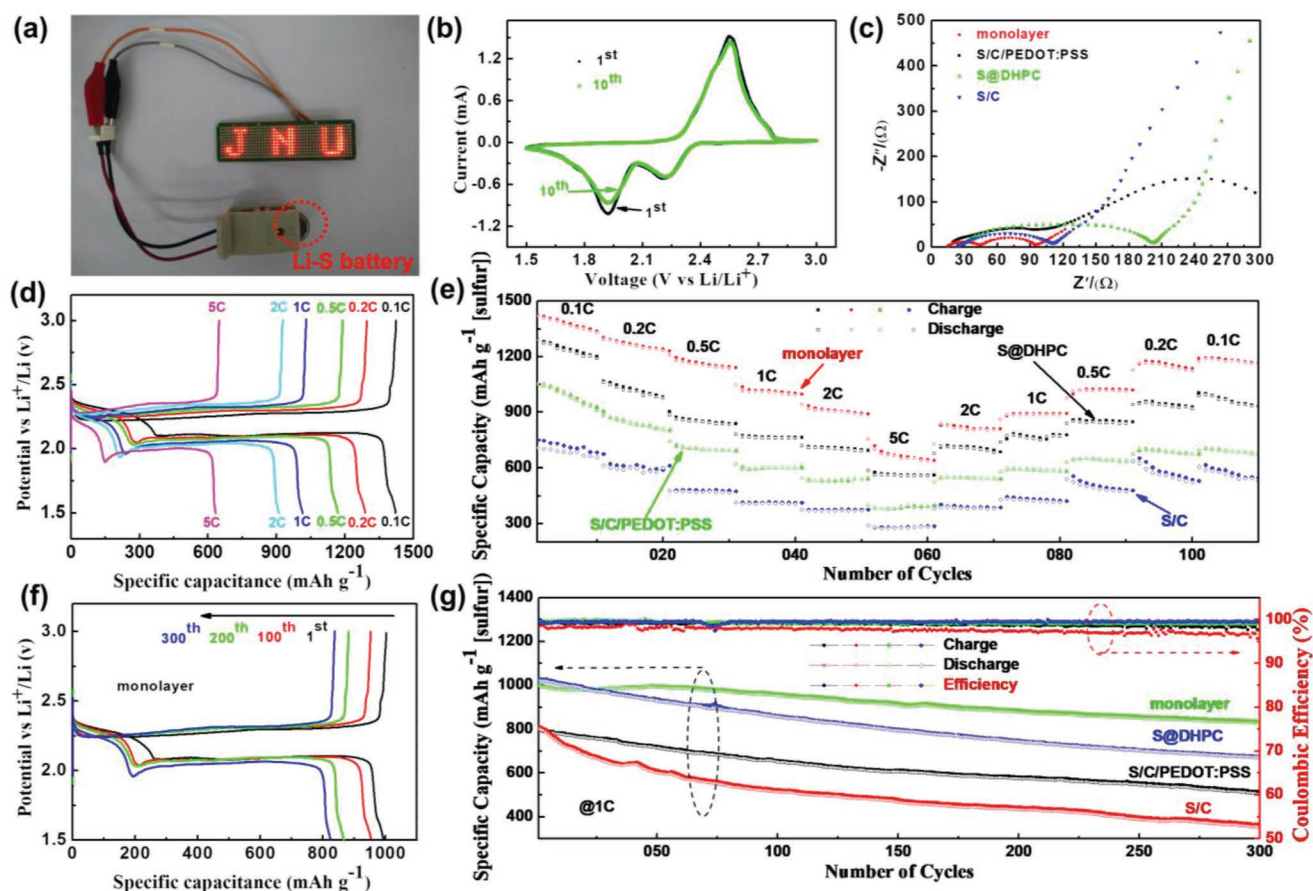
Figure 4. a) Photograph of LEDs that are powered by a button-type Li-S battery with the S@DHPC/PEDOT:PSS monolayer electrode. b) CV curves of the S@DHPC/PEDOT:PSS monolayer electrode at the scan rate of 0.1 mV s^{-1}. c) Nyquist plots for the S@DHPC/PEDOT:PSS monolayer electrode, S@DHPC, S/C, and S/C/PEDOT:PSS electrodes. d) Charge–discharge profiles of the S@DHPC/PEDOT:PSS monolayer electrode at different rate densities. e) Rate performance of the S@DHPC/PEDOT:PSS monolayer electrode, S@DHPC, S/C, and S/C/PEDOT:PSS electrodes at various current density. f) Charge–discharge profiles of the S@DHPC/PEDOT:PSS monolayer electrode in different cycles. g) Cycling performance of S@DHPC/PEDOT:PSS monolayer electrode, S@DHPC, S/C, and S/C/PEDOT:PSS electrodes at the current density of 1 C.

S@DHPC/PEDOT:PSS monolayer electrode was fabricated, which was able to light "JNU"-shaped light-emitting diodes (LEDs) (**Figure 4**a). The LEDs stayed on for over 8 h, indicating a high capacity of the battery. To elucidate the benefits of the S@DHPC layer framework in the electrode, the electrochemical behavior of the monolayer electrode was examined by cyclic voltammetric (CV) and electrochemical impedance spectroscopy (EIS) measurements. From Figure 4b, the CV curves can be seen to show two peaks in the cathodic scan and one in the anodic scan, which may be ascribed to the redox reaction of conversion of S_8 ring to high-order polysulfides (Li_2S_n, $4 \leq n \leq 8$) and further reduction of polysulfides to sulfides (Li_2S) for the discharging state. The anodic peak at about 2.54 V can be ascribed to the oxidation of Li_2S to pure sulfur.[30] In addition, the fact that the first and tenth cycles show an almost perfect overlap indicates excellent cycling stability of the monolayer electrode. The interfacial impedance of the series of electrodes was then evaluated by electrochemical impedance analysis. Figure 4c depicts the Nyquist plots of the impedance spectra of the S@DHPC/PEDOT:PSS monolayer electrode, S@DHPC, S/C, and S/C/PEDOT:PSS electrodes.

These electrodes all exhibit one or two semicircles in the high-frequency region along with a radial oblique line in the low-frequency region, from which the charge-transfer resistance (R_{ct}) and semi-infinite ion Warburg (W_0) diffusion impedance can be quantitatively evaluated.[31] Among these, the S@DHPC/PEDOT:PSS monolayer electrode exhibited the lowest R_{ct} (79.3 Ω) (Figure S4, Table S1, Supporting Information). It should be noted that the semicircular radii in the Nyquist plots of the bilayer electrode and trilayer electrode were almost identical, indicating that the electron-transfer kinetics was not compromised with a higher loading of the cathode materials likely because of the incorporation of conducting polymers.

Charge–discharge experiments were then carried out to evaluate the electrochemical performance of the monolayer electrode at various current densities from 0.1 to 5 C (Figure 4d,e). The monolayer electrode is found to deliver a capacity of 1420 mAh g^{-1} at 0.1 C, 1288 mAh g^{-1} at 0.2 C, 1170 mAh g^{-1} at 0.5 C, 1014 mAh g^{-1} at 1 C, 912 mAh g^{-1} at 2 C, and 626 mAh g^{-1} at 5 C. The corresponding charge–discharge profiles of the other electrodes are shown in Figure S5 (Supporting Information). These results suggest that the monolayer electrode delivers

**ADVANCED
SCIENCE NEWS**
www.advancedsciencenews.com

**small
methods**
www.small-methods.com
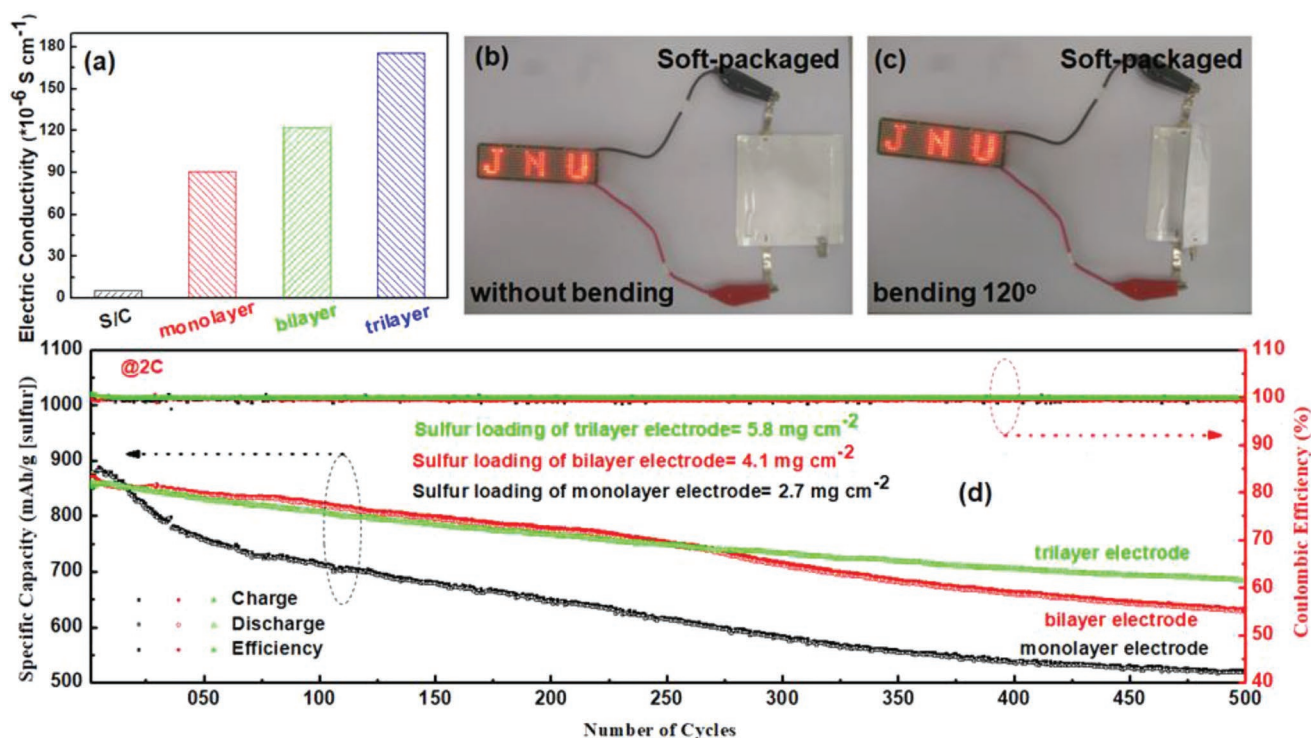
Figure 5. a) Bar chart of the electrical conductivity of the S/C electrode, S@DHPC/PEDOT:PSS monolayer electrode, bilayer electrode, and trilayer electrode. b,c) LEDs lit by a soft-packaged Li-S battery using the trilayer electrode without bending and under 120° bending. d) Cycle performance of the S@DHPC/PEDOT:PSS monolayer electrode, bilayer electrode, and trilayer electrode at 2 C.

the highest reversible capacities among the series, where the excellent rate capability is most likely due to the 3D hierarchical porous framework of DHPC and coating of conducting polymer films. Moreover, the monolayer electrode exhibits good cycling stability, as shown in Figure 4f,g. At the current density of 1 C, the reversible capacities of the monolayer electrode retained 83.18% of the specific capacity at 826 mAh g^{-1} after 300 cycles, corresponding to a capacity diminishment of only 0.0634% cycle^{-1}, while the capacity of the S@DHPC, S/C, and S/C/PEDOT:PSS electrodes diminished rapidly to 672, 502, and 353 mAh g^{-1} after 300 cycles, corresponding to a much higher fading rate of 0.1397, 0.1151, and 0.2732% cycle^{-1}, respectively (Figure S6, Supporting Information).

The corresponding energy efficiency follows a similar trend.[32] From Figure 4f and Figure S6 (Supporting Information), the energy efficiency was estimated to be 91.7% for the S@DHPC/PEDOT:PSS electrode, 91.5% for S@DHPC, 89.6% for S/C/PEDOT:PSS, and 88.9% for S/C electrode. The high energy efficiency for the monolayer electrode and S@DHPC electrode is most likely due to fast electron transfer and ion diffusion in DHPC which reduced electrode polarization. Taken together, these results indicate that the 3D hierarchical porous structure played a significant role in improving the cycling performance.

In addition, one can see that coating of the electrode with a conducting polymer layer (i.e., S@DHPC/PEDOT:PSS monolayer electrode and S/C/PEDOT:PSS electrode) led to a lower capacity attenuation, indicating that the coating layer served as a protective layer that effectively impeded the

diffusion/dissolution of polysulfides into the electrolyte. Notably, the electrode performance can be further enhanced by increasing the number of the S@DHPC/PEDOT:PSS layer. **Figure 5**a depicts the electrical conductivity of the S/C electrode, S@DHPC/PEDOT:PSS monolayer electrode, bilayer electrode, and trilayer electrode, as determined by two-probe measurements. It can be seen that the electrical conductivity for S/C was estimated to be 2.35×10^{-6} S cm^{-1}, which increased markedly to 9×10^{-5} S cm^{-1} for the monolayer electrode, further to 1.2×10^{-4} S cm^{-1} for the bilayer electrode and 1.8×10^{-4} S cm^{-1} for the trilayer electrode.

To demonstrate the flexibility of the trilayer electrode, two soft-packaged Li-S batteries were fabricated, as shown in Figure S7 (Supporting Information), and used to light the LEDs mentioned above. The LEDs remained on even when the soft-packaged Li-S batteries were bent by 120° (Figure 5b,c), indicating excellent mechanical flexibility of the trilayer electrode. Furthermore, the long cycle performance of the S@DHPC/PEDOT:PSS monolayer electrode, bilayer electrode, and trilayer electrode also revealed that the highly conductive PEDOT:PSS coating films can significantly enhance cycling stability of the electrodes (Figure 5d). In particular, the trilayer electrode delivered a discharge capacity of 846 mAh g^{-1} in the first cycle and retained 716 mAh g^{-1} after 500 cycles, corresponding to a fading rate of only 0.033% cycle^{-1}, in comparison to 0.085 and 0.053% cycle^{-1} for the monolayer electrode and bilayer electrode. By contrast, the S/C electrode retained only 52.1% of the capacity at 349 mAh g^{-1} after only 300 cycles (Figure S8, Supporting Information), corresponding to a much

higher fading rate of 0.218% cycle^{-1}. The fact that the fading rates of the monolayer, bilayer, and trilayer electrodes were almost one order of magnitude lower than that of the S/C electrode indicates that the PEDOT:PSS films effectively impeded the dissolution and diffusion of polysulfides into the electrode. Table S2 (Supporting Information) lists the electrochemical performance of Li-S batteries in recent literature, where one can see that high sulfur loading and good cycling stability in general cannot be achieved simultaneously, as a high sulfur loading typically leads to an increase of polysulfide dissolution. Yet, the trilayer electrode prepared above actually exhibited significant improvement in cycling stability despite a high sulfur loading of 5.8 mg cm^{-2}. This is most likely due to the compartmentation of sulfur by the PEDOT:PSS polymer layers in the unique layer architecture of the electrode (Figure 1).

The surface morphologies of the S/C and trilayer electrode before and after cycling tests are then evaluated and compared, as shown in **Figure 6**. The trilayer electrode can be seen to exhibit a convex structure on the PEDOT:PSS surface, which becomes more apparent after cycling, whereas the S/C electrode displays a porous structure on the surface with the diameters of the holes ranging from sub-micrometer to several

micrometers after 500 cycles. Consistent results were obtained from the SEM images of the cross section of the S/C electrode (Figure S9a,b, Supporting Information). By contrast, no obvious change of the structural morphologies was observed with the trilayer electrode before and after cycling tests (Figure S9c,d, Supporting Information). In addition, XPS studies (Figure S10, Supporting Information) showed that the sulfur content in the freshly prepared trilayer electrode was ≈64 wt%, and dropped to 54% after 500 cycles, whereas it declined much more rapidly from 67 to 32 wt% after only 300 cycles with the S/C electrode. These results indicate that indeed a polymer coating layer can effectively impede the loss of polysulfides into electrolyte.

The influence of a polymer interlayer on polysulfide diffusion in Li-S batteries was also examined by using a U-shape electrolyzer.[33] As shown in **Figure 7**, a PEDOT:PSS-capped diaphragm or regular diaphragm was inserted between two plastic spacers to separate the U-shape electrolyzer into two compartments. Initially, the color of the left compartment is dark yellow because of polysulfides in the electrolyte, whereas the right compartment is colorless with only the electrolyte. After 1 h of operation, the right compartment remained colorless with the PEDOT:PSS-capped diaphragm, whereas a light yellow color
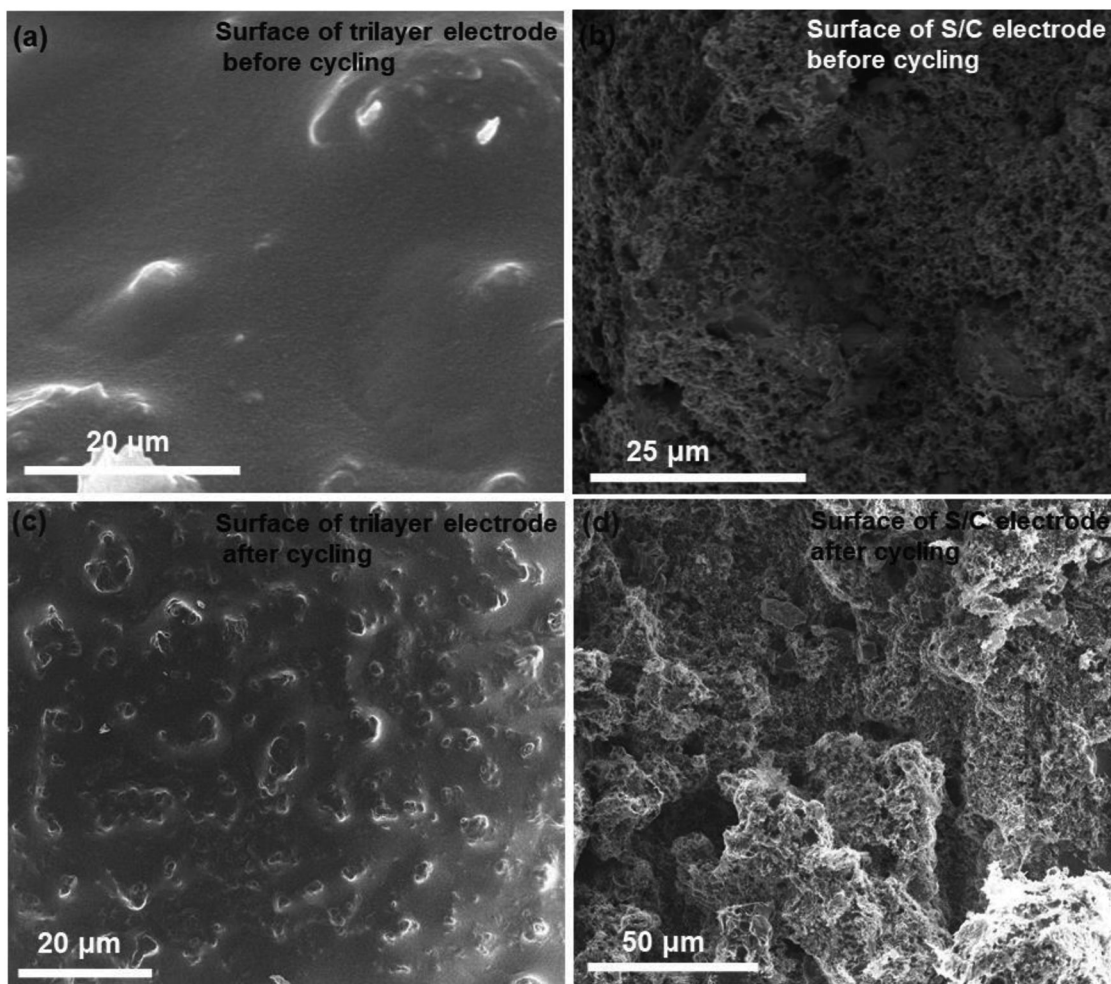
Figure 6. a,c) SEM images of the trilayer electrode before cycling and after 500 charge–discharge cycles at 2 C. b,d) SEM images of the S/C electrode before cycling and after 500 charge–discharge cycles at 2 C.
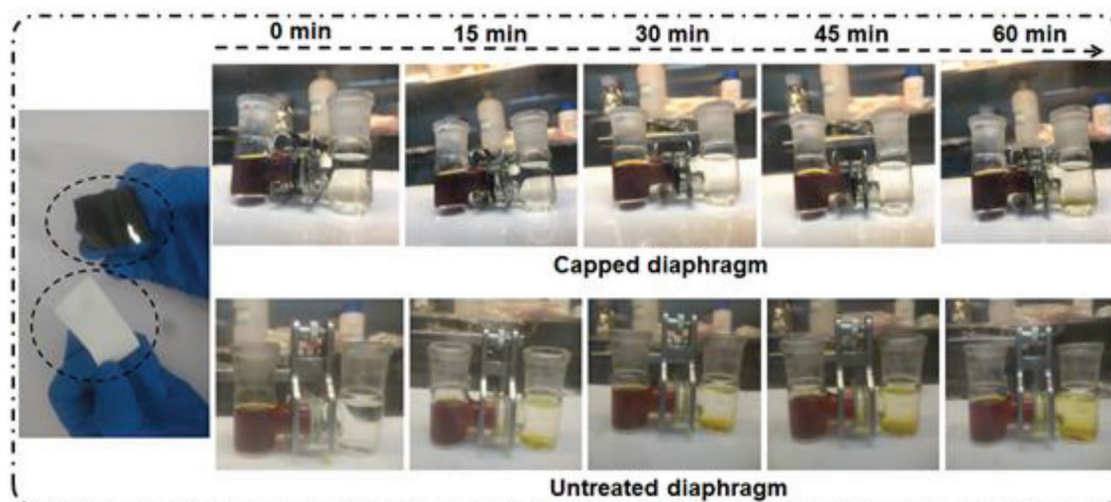
Figure 7. Demonstration of the blocking of the diffusion of polysulfides by (top panels) PEDOT:PSS-capped diaphragm and (bottom panels) untreated diaphragm. The left compartment of the electrolyzer is filled with the electrolyte containing 3 mol L^{-1} polysulfides, and the right compartment is filled with blank electrolyte only.

started to appear with the untreated diaphragm, and the contrast became even more pronounced at longer reaction times (up to 3 d, Figure S11, Supporting Information). This suggests that the PEDOT:PSS polymer layer indeed can effectively impede the diffusion of polysulfides.

3. Conclusion

In summary, a sulfur cathode (S@DHPC) was prepared by infiltrating sulfur into a 3D hierarchical porous carbon scaffold. Coating of the S@DHPC electrode with PEDOT:PSS conducting polymers was found to effectively improve the electrochemical performance of the electrode. This was ascribed to the high porosity of the DHPC matrix that facilitated the encapsulation of sulfur. More importantly, the PEDOT:PSS capping layers impeded the diffusion/loss of polysulfides, leading to improved cycling stability of the electrode. With a high sulfur loading density of 5.8 mg cm^{-2}, the trilayer electrode delivered a discharge capacity of 846 mAh g^{-1} in the first cycle and retained 716 mAh g^{-1} after 500 cycles, corresponding to a fading rate of only 0.033% cycle^{-1}. These results suggest that a layered architecture of S@DHPC/PEDOT:POSS may be exploited for the preparation of effective cathode materials of high-performance Li-S batteries.

4. Experimental Section

Preparation of S@DHPC and Multilayer Electrodes: Polypyrrole (PPy) precursor was synthesized by adopting a literature procedure based on oxidative template assembly.[34] First, 2.5 g of cetrimonium bromide ((C$_{16}$H$_{33}$)N(CH$_3$)$_3$Br) was dissolved in 50 mL of a HCl solution (1 mol L^{-1}) in an ice bath, into which was then added 5.2 g of ammonium persulfate, yielding a pale yellow solution. 5.4 mL of pyrrole monomers was then added into the template solution. After the completion of the reaction, a precipitate was formed, which was collected and washed with a HCl solution (0.2 mol L^{-1}) and deionized water three times, affording PPy that was dried overnight at 60 °C in an oven.

DHPC was prepared via a chemical activation route with the obtained PPy as precursors and KOH as the activating reagent. Briefly, 3 g of PPy prepared above was added into 50 mL KOH (8 mol L^{-1}) solution under magnetic stirring to form a black slurry, which was then collected and subject to a thermal treatment under a N$_2$ atmosphere at the heating rate of 10 °C min^{-1} to 700 °C for 2 h, producing DHPC.[34] The S@DHPC composite was prepared by melt immersion at high pressures, where a mixture of sulfur and DHPC was loaded into a stainless steel autoclave and sealed with a Swagelok structure cover. The autoclave was heated at 155 °C for 5 h before the temperature was increased to 300 °C and kept for 5 h to guarantee that the melted sulfur was completely infiltrated into the DHPC pores under the autogenerated pressure.

The S@DHPC electrodes were prepared by a doctor blade coating method.[35] In brief, polyvinylidene fluoride (PVDF) binder was dissolved in N-methyl-2-pyrrolidone (NMP) under magnetic stirring. The obtained S@DHPC and commercial Super P carbon were added into the solution to form a homogenous slurry at the mass ratio of S@DHPC:Super P carbon:PVDF = 80:10:10. The above slurry was then cast onto an aluminum current collector with a thickness of 100 μm and dried at 60 °C for 12 h. The electrode was then coated with a thin film of PEDOT:PSS (purchased from Luoyang Weiguang Electronic Technology Co. Ltd.) by a simple drip coating method, affording S@DHPC/PEDOT:PSS monolayer electrode. The same procedure was repeated to prepare the bilayer and trilayer electrodes. The corresponding mass loading of sulfur was estimated to be 2.7, 4.1 mg, and 5.8 mg cm^{-2}, respectively. Conventional S/C electrodes with and without PEDOT:PSS coating, at a sulfur loading of 2.35 mg cm^{-2}, were also prepared in the same fashion for comparison.

Button-Cell Fabrication and Battery Tests: Button cells (CR2032) were assembled in an Ar-filled glove box. The cell was comprised of a positive electrode, diaphragm, lithium wafers, and electrolyte. A Celgard 2400 diaphragm served as the separator, lithium wafers as the reference and/or counter electrode, and a mixed solution of 1,3-dioxolane and 1,2-dimethoxyethane (v:v 1:1) containing 1 M lithium bis(trifluromethanesulfonyl)imide (LiTFSI) as the electrolyte. Galvanostatic discharge–charge tests on the fabricated cells were performed with a cell test system (LANHE CT2001A 5 V 20 mA). CV studies were performed in the potential range of 1.5–3.0 V. EIS studies were carried out at the charged state within the frequency range of 100 kHz to 10 mHz at an AC amplitude of 5 mV.

Materials Characterization: SEM measurements were conducted on a FEI field emission scanning electron microscope at the acceleration voltage of 5.0 kV. XPS measurements were carried out on a Phi X-tool

XPS instrument. XRD measurements were performed on Bruker D8 using Cu Kα radiation. TGA was conducted on a METTLER instrument in a N$_2$ atmosphere at the heating rate of 10 °C min^{-1}. Raman spectra were recorded on a RENISHAW instrument with an Ar laser of 488 nm. The surface area, total pore volume, and pore size distribution analysis were performed with a Quantachrom Autosorb equipment using the BET method. For electrical conductivity measurements, the electrodes were sliced to circular sheets of the same diameter. Then the electric conductivity was measured on a Keithley 2636B source meter.

Supporting Information

Supporting Information is available from the Wiley Online Library or from the author.

Acknowledgements

Conflict of Interest

The authors declare no conflict of interest.

Keywords

[1] J. Cai, C. Wu, Y. Zhu, K. Zhang, P. K. Shen, *J. Power Sources* **2017**, *341*, 165.

[2] a) H. Wang, W. Zhang, H. Liu, Z. Guo, *Angew. Chem., Int. Ed.* **2016**, *55*, 3992; b) A. Eftekhari, D. W. Kim, *J. Mater. Chem. A* **2017**, *5*, 17734.

[3] a) Z. Ma, Z. Li, K. Hu, D. Liu, J. Huo, S. Wang, *J. Power Sources* **2016**, *325*, 71; b) H. Lin, S. Zhang, T. Zhang, H. Ye, Q. Yao, G. W. Zheng, J. Y. Lee, *Adv. Energy Mater.* **2018**, *8*, 1801868.

[4] N. Osada, C. B. Bucur, H. Aso, J. Muldoon, *Energy Environ. Sci.* **2016**, *9*, 1668.

[5] F. Pei, L. Lin, D. Ou, Z. Zheng, S. Mo, X. Fang, N. Zheng, *Nat. Commun.* **2017**, *8*, 482.

[6] D. Wang, W. Zhang, W. Zheng, X. Cui, T. Rojo, Q. Zhang, *Adv. Sci.* **2017**, *4*, 1600168.

[7] H. Zhang, Q. Gao, W. Qian, H. Xiao, Z. Li, L. Ma, X. Tian, *ACS Appl. Mater. Interfaces* **2018**, *10*, 18726.

[8] G. Zhang, Z. W. Zhang, H.-J. Peng, J.-Q. Huang, Q. Zhang, *Small Methods* **2017**, *1*, 1700134.

[9] a) P. Wu, L. H. Chen, S. S. Xiao, S. Yu, Z. Wang, Y. Li, B. L. Su, *Nanoscale* **2018**, *10*, 11861; b) Z. Liu, X. Zheng, N. Y. Yuan, J. N. Ding, *J. Mater. Chem. A* **2017**, *5*, 942.

[10] Y. Hou, J. Li, X. Gao, Z. Wen, C. Yuan, J. Chen, *Nanoscale* **2016**, *8*, 8228.

[11] G. Hu, Z. Sun, C. Shi, R. Fang, J. Chen, P. Hou, C. Liu, H. M. Cheng, F. Li, *Adv. Mater.* **2017**, *29*, 1603835.

[12] L. Li, G. Zhou, L. Yin, N. Koratkar, F. Li, H. M. Cheng, *Carbon* **2016**, *108*, 120.

[13] a) H. S. Kang, Y. K. Sun, *Adv. Funct. Mater.* **2016**, *26*, 1225; b) X. Li, A. Lushington, Q. Sun, W. Xiao, J. Liu, B. Wang, Y. Ye, K. Nie, Y. Hu, Q. Xiao, R. Li, J. Guo, T. K. Sham, X. Sun, *Nano Lett.* **2016**, *16*, 3545.

[14] S. H. Chung, P. Han, R. Singhal, V. Kalra, A. Manthiram, *Adv. Energy Mater.* **2015**, *5*, 1500738.

[15] a) X. Jia, C. Zhang, J. Liu, W. Lv, D. W. Wang, Y. Tao, Z. Li, X. Zheng, J. S. Yu, Q. H. Yang, *Nanoscale* **2016**, *8*, 4447; b) J. He, Y. Chen, W. Lv, K. Wen, P. Li, F. Qi, Z. Wang, W. Zhang, Y. Li, W. Qin, W. He, *J. Power Sources* **2016**, *327*, 474; c) H. Lin, L. Yang, X. Jiang, G. Li, T. Zhang, Q. Yao, G. W. Zheng, J. Y. Lee, *Energy Environ. Sci.* **2017**, *10*, 1476.

[16] X. Fang, W. Weng, J. Ren, H. Peng, *Adv. Mater.* **2016**, *28*, 491.

[17] Z. Du, J. Xu, S. Jin, Y. Shi, C. Guo, X. Kong, Y. Zhu, H. Ji, *J. Power Sources* **2017**, *341*, 139.

[18] G. Li, J. Sun, W. Hou, S. Jiang, Y. Huang, J. Geng, *Nat. Commun.* **2016**, *7*, 10601.

[19] S. H. Chung, C. H. Chang, A. Manthiram, *Energy Environ. Sci.* **2016**, *9*, 3188.

[20] Z. W. Seh, W. Li, J. J. Cha, G. Zheng, Y. Yang, M. T. McDowell, P. C. Hsu, Y. Cui, *Nat. Commun.* **2013**, *4*, 1331.

[21] L. Qie, A. Manthiram, *Adv. Mater.* **2015**, *27*, 1694.

[22] R. J. Chen, T. Zhao, J. Lu, F. Wu, L. Li, J. Z. Chen, G. Q. Tan, Y. S. Ye, K. Amine, *Nano Lett.* **2013**, *13*, 4642.

[23] a) J. Xu, J. Ma, Q. Fan, S. Guo, S. Dou, *Adv. Mater.* **2017**, *29*, 1606454; b) S. Zeng, L. Li, L. Xie, D. Zhao, N. Wang, S. Chen, *ChemSusChem* **2017**, *10*, 3378.

[24] H. Cheng, S. Wang, *J. Mater. Chem. A* **2014**, *2*, 13783.

[25] S. Zeng, L. Li, D. Zhao, J. Liu, W. Niu, N. Wang, S. Chen, *J. Phys. Chem. C* **2017**, *121*, 2495.

[26] N. Xu, T. Qian, X. Liu, J. Liu, Y. Chen, C. Yan, *Nano Lett.* **2017**, *17*, 538.

[27] H. Kim, J. Lee, H. Ahn, O. Kim, M. J. Park, *Nat. Commun.* **2015**, *6*, 7278.

[28] K. Park, J. H. Cho, J. H. Jang, B. C. Yu, A. T. De La Hoz, K. M. Miller, C. J. Ellison, J. B. Goodenough, *Energy Environ. Sci.* **2015**, *8*, 2389.

[29] Y. Zhong, X. Xia, S. Deng, J. Zhan, R. Fang, Y. Xia, X. Wang, Q. Zhang, J. Tu, *Adv. Energy Mater.* **2018**, *8*, 1701110.

[30] M. Wang, H. Zhang, W. Zhou, X. Yang, X. Li, H. Zhang, *J. Mater. Chem. A* **2016**, *4*, 1653.

[31] X. Gu, C. Tong, C. Lai, J. Qiu, X. Huang, W. Yang, B. Wen, L. Liu, Y. Hou, S. Zhang, *J. Mater. Chem. A* **2015**, *3*, 16670.

[32] A. Eftekhari, *Sustainable Energy Fuels* **2017**, *1*, 2053.

[33] H. Tang, S. Yao, S. Xue, M. Liu, L. Chen, M. Jing, X. Shen, T. Li, K. Xiao, S. Qin, *Electrochim. Acta* **2018**, *263*, 158.

[34] L. Qie, W. Chen, H. Xu, X. Xiong, Y. Jiang, F. Zou, X. Hu, Y. Xin, Z. Zhang, Y. Huang, *Energy Environ. Sci.* **2013**, *6*, 2497.

[35] G. Ai, Z. Wang, H. Zhao, W. Mao, Y. Fu, R. Yi, Y. Gao, V. Battaglia, D. Wang, S. Lopatin, G. Liu, *J. Power Sources* **2016**, *309*, 33.